

# Supplementary Information for Optimizing Iodide-Adduct CIMS Quantitative Method for Toluene Oxidation Intermediates: Experimental Insights into Functional Group Differences

Mengdi Song<sup>1,3</sup>, Shuyu He<sup>1,3</sup>, Xin Li<sup>1,2,3</sup>, Ying Liu<sup>1,3</sup>, Shengrong Lou<sup>4</sup>, Sihua Lu<sup>1,3</sup>, Limin Zeng<sup>1,3</sup>, and Yuanhang Zhang<sup>1,3</sup>

<sup>1</sup>State Key Joint Laboratory of Environmental Simulation and Pollution Control, College of Environmental Sciences and Engineering, Peking University, Beijing, 100871, P.R. China

<sup>2</sup>Collaborative Innovation Center of Atmospheric Environment and Equipment Technology, Nanjing University of Information Science & Technology, Nanjing, 210044, P.R. China

<sup>3</sup>International Joint Laboratory for Regional Pollution Control, Ministry of Education, Beijing, 100816, P.R. China

<sup>4</sup>State Environmental Protection Key Laboratory of Formation and Prevention of Urban Air Pollution Complex, Shanghai Academy of Environmental Sciences, Shanghai, 200233, P.R. China

Correspondence to: Xin Li (li\_xin@pku.edu.cn)

## Contents

Section S1. Semi-Quantitative Methods Based on Voltage scanning.....	S-2
Section S2. Additional Measurements Conducted During Chamber Experiments.....	S-2
Section S3. <i>k</i> -Means Cluster analysis.....	S-2
Section S4. Humidity correction analysis.....	S-3
Table S1. Detailed information on the direct calibration of species associated with aromatic hydrocarbons and their oxidation products in this study.....	S-4
Figure S1. Schematic diagram of the chamber set up for the aromatic hydrocarbon oxidation experiment.....	S-6
Figure S2. Comparison of the sensitivity of species containing different functional groups in (a) this study, (b) Lee et al., and (c) Ye et al. ....	S-7
Figure S3. Criterion values for number of clusters from 2 to 8.....	S-8
Figure S4. The effect of humidity on the sensitivity of I-CIMS.....	S-9
Figure S5. I-CIMS mass transmission efficiency based on direct calibration species.....	S-10
Figure S6. Fitting curve for cluster binding enthalpies and logarithmic sensitivities at PBE/SDD, PBE/SDD (D3), and B3LYP/Def2TZVP (D3) level.....	S-11
Figure S7. The application of classification-based semi-quantitative methods in previous studies (Iyer et al., 2016) .....	S-12
Figure S8. The difference between the measured sensitivity and the calculated sensitivity at the B3LYP/Def2TZVP (D3) level in this study.....	S-13
Figure S9. The schematic diagram of the oxidation intermediates in the toluene + OH system.....	S-14
Figure S10. Fitting results of the relative binding energy indicator $dV_{50}$ for the iodide adducts of standard species and aromatic hydrocarbon oxidation products with the species sensitivity relative to maximum sensitivity, where $dV_{50}$ represents the voltage at half signal maximum.....	S-15
Figure S11. Time series of (a) glyoxal and (b) methyl glyoxal during the oxidation of toluene without NO injection (blue) and with NO injection (orange).....	S-16

## Section S1 Semi-Quantitative Methods Based on Voltage scanning

The second semi-quantitative method for the I-CIMS instrument is based on the voltage scanning method proposed by Lopez-Hilfiker et al. (Lopez-Hilfiker et al., 2016). After a declustering scan for iodine addition was performed, the correlation between the voltage difference  $dV_{50}$  at which half of the signal was removed and the sensitivity of iodine addition was analysed. In this study, we show the fitting results of the relative binding energy indicator  $dV_{50}$  of the iodide adducts of standard species and aromatic hydrocarbon oxidation products with the species sensitivity relative to maximum sensitivity ( $1/S_0$ ), which has sigmoidal characteristics; the  $R^2$  value was 0.8909 (Figure S10). The sensitivity of nonstandard species could be quantitatively analysed by multiplying the  $1/S_0$  obtained by the semi-dissociation voltage with the maximum sensitivity ( $S_{\max}$ ) of the instrument. (Ye et al., 2021) Multiplying  $S_{\max}$  by  $1/S_0$  is defined as reference sensitivity.

The detailed semi-quantitative expression based on voltage scanning, is shown in Formula S1:

$$[X_{\text{ppb}}] = \frac{\text{Normalized signal}}{\left(S_{\max} \times \frac{1}{S_0}\right) \times \text{MassTrans} \times \text{RH}_{\text{Corr}}} \quad (\text{S1})$$

where  $S_{\max}$  represents the empirical maximum sensitivity;  $1/S_0$  represents the species sensitivity relative to the maximum sensitivity; MassTrans represents the mass transmission correction equation; and  $\text{RH}_{\text{Corr}}$  represents the humidity correction equation.

## Section S2 Additional Measurements Conducted During Chamber Experiments

An Ionicon proton-transfer-reaction quadrupole mass spectrometry (PTR-QMS) instrument was used to measure nonmethane hydrocarbons (HMHCs), aldehydes (benzaldehyde, etc.), and other oxidation products that could not be measured by I-CIMS. PTR-QMS uses  $\text{H}_3\text{O}^+$  as the ion source. In a drift tube, aromatic hydrocarbon oxidation intermediates (X) that have high proton affinity can undergo a proton transfer reaction with  $\text{H}_3\text{O}^+$  to form the product ion ( $\text{XH}^+$ ) (Yuan et al., 2017).  $\text{XH}^+$  is then detected by the mass spectrometry detector. HMHCs and some oxidation products were calibrated using gas standards and penetrant tubes under experimental conditions. The signals measured by PTR-QMS were normalized using the sum of 500 times  $\text{H}_3[^{18}\text{O}]^+$  and 250 times  $\text{H}_2\text{O}(\text{H}_3[^{18}\text{O}])^+$  reagent ions at  $10^6$  cps (Huang et al., 2019). The linear correlation between the signal values and calibrated species concentrations had an  $R^2$  value greater than 0.99 for all species. The sensitivities of acetonitrile, toluene, m-cresol, and benzaldehyde at 30% (60%) humidity were 17.59 (16.66) ncps/ppb, 10.55 (9.75) ncps/ppb, 13.08 (10.61) ncps/ppb and 16.14 (15.24) ncps/ppb, respectively. Glyoxal and methyl glyoxal were measured by a home-built Incoherent BroadBand Cavity Enhanced Absorption Spectroscopy (IBBCEAS) instrument (Liu et al., 2019; Liu et al., 2021). The detection limits for glyoxal and methyl glyoxal were 30 ppt and 100 ppt, respectively, at 100 s time resolution. Formaldehyde and  $\text{H}_2\text{O}$  were measured by a commercial cavity ringdown instrument (PICARRO G2307) with detection limits of 0.3 ppb at a 1 min time resolution.  $\text{NO}_x$  was measured by a commercial chemiluminescence technology instrument (Thermo Scientific™ Model 42i) with detection limit of 0.4 ppb at a 1 min time resolution.  $\text{O}_3$  was measured by a nondispersive ultraviolet (UV) absorption technology instrument (ECOTECH 9810<sub>series</sub>) with a detection limit of 0.5 ppb at a 1 min time resolution. Temperature and humidity were measured by commercial sensor instruments (R5000C, Sinomeasure, China).

## Section S3 *k*-Means Cluster analysis

Machine learning is gradually becoming an emerging and significant analytical method in the field of environmental science research (Zhong et al., 2021). This study employs *k*-means cluster analysis to classify the humidity response curves during the calibration process, establishing

a humidity-corrected equation for sensitivity. *k*-Means cluster analysis is a widely used unsupervised machine learning algorithm that aims to partition a dataset into a predetermined number of clusters (Äijälä et al., 2017; Zhong et al., 2021). It is an iterative clustering algorithm, with the following steps: first, the data is divided into *k* groups; then, *k* objects are randomly selected as the initial cluster centres. Next, the distance between each object ( $x_i$ ) in each cluster  $C_n$  and its cluster centre ( $\mu_n$ ) is calculated (as in Equation 5) (Äijälä et al., 2017). Through repeated iterations, each object is assigned to the nearest cluster centre, minimizing the sum of distances for all clusters  $C_n$  to determine the optimal result.

$$J(C_n) = \sum_{x \in C_n} \|x_i - \mu_n\|^2 \quad (\text{S2})$$

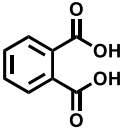
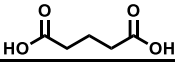
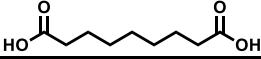
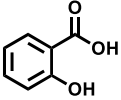
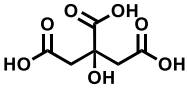
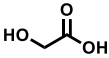
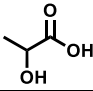
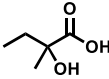
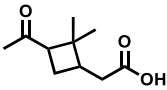
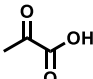
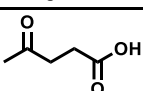
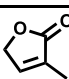
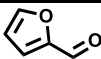
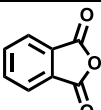
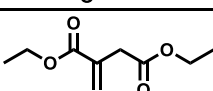
#### Section S4 Humidity correction analysis

Humidity has a significant influence on the sensitivity of iodine adducts (Ye et al., 2021; Lee et al., 2014). The influence of humidity on the sensitivity of a given compound mainly manifests in two ways (Lee et al., 2014): (1) Positive influence: When the introduction of water vapor stabilizes the iodide-adduct cluster, the sensitivity of the compound increases; (2) Negative effect: When the introduction of water vapor enhances the binding of iodide ions to form  $\text{H}_2\text{OI}$ , the sensitivity of the compound decreases. Therefore, different types of species respond differently to the effects of humidity. Employing *k*-means cluster analysis on sensitivity changes across functional groups with humidity (section S3), we identified an optimal cluster number of 4 out of 2 to 8 options, as shown in Figure S3. Consequently, sensitivity was categorized into four groups for humidity correction analysis, as depicted in Figure S4.

The first category was compounds containing single active functional group. The main representative species were acrylic acid ( $\text{C}_3\text{H}_4\text{O}_2\text{I}$ ), propionic acid ( $\text{C}_3\text{H}_6\text{O}_2\text{I}$ ), and *m*-cresol ( $\text{C}_7\text{H}_8\text{OI}$ ). The first category of species exhibited lower sensitivity and was notably influenced by water molecules competing for  $\text{I}^-$ . As a result, the sensitivity of these species exhibited a significant and rapid decline with increasing humidity (Figure S4e – g). The parameterized equation for sensitivity and humidity of the second category of compounds conformed to the Boltzman function, and the correlation  $R^2$  of the fitting curve reached a value of 0.98 (Figure S4a). The second category consisted of compounds containing multiple active functional groups, and the main representative species were oxalic acid ( $\text{C}_2\text{H}_2\text{O}_4\text{I}$ ) and pinonic acid ( $\text{C}_{10}\text{H}_{16}\text{O}_3\text{I}$ ). The sensitivity of active functional groups of the second-category species was higher than that of the first-category species, and the effect of the competition of water molecules for  $\text{I}^-$  was weakened. The sensitivity of these compounds decreased significantly and slowly with an increase in humidity (Figure S4h – i). The parameterized equation for sensitivity and humidity for the third category of compounds conformed to a one basic exponential (ExpDec1) function, and the correlation  $R^2$  for the fitting curve reached a value of 0.92 (Figure S4b). The third group consisted of polyphenol compounds, and the main representative species were 2,4-Dihydroxytoluene ( $\text{C}_7\text{H}_8\text{O}_2\text{I}$ ) and 2,4,6-trihydroxytoluene ( $\text{C}_7\text{H}_8\text{O}_3\text{I}$ ). The third -category species had strong capacities to bind to iodide ions and were nearly unaffected by humidity. Their sensitivity did not change significantly with an increase in humidity (Figure S4c). The fourth category consisted of small-molecular-weight acid compound and it was mainly represented by formic acid ( $\text{CH}_2\text{O}_2\text{I}$ ). Theoretical studies have confirmed that the presence of water molecules can enhance the stability of  $\text{CH}_2\text{O}_2$  binding to  $\text{I}^-$  at low humidity (Lee et al., 2014). Therefore, the sensitivity of  $\text{CH}_2\text{O}_2\text{I}$  increased by approximately two times when the humidity ranged from 0 to 2 mmol/mol (Figure S4d). When the humidity exceeded 2 mmol/mol, the increased water molecules captured  $\text{I}^-$  to bind with  $\text{H}_2\text{OI}$ , which reduced the sensitivity of  $\text{CH}_2\text{O}_2\text{I}$ . The parametric equation of sensitivity and humidity of formic acid was consistent with an asymmetric double sigmoidal (Asym2Sig) function, and the correlation  $R^2$  of the fitting curve was about 1.00 (Figure S4d). By establishing these classifications for humidity-dependent parametric equations, we could calibrate the measured signals of each species to obtain actual concentration data. Moreover, the humidity correction of species for which standard samples were not available could be estimated based on the characteristics of similar species.

**Table S1: Detailed information on the direct calibration of species associated with aromatic hydrocarbons and their oxidation products in this study.**

Type	No.	Species	Formula	MW	Detection limit*	Structure
Monophenol	1	m-Cresol	C <sub>7</sub> H <sub>8</sub> O	108.06	0.083	
	2	Phenol	C <sub>6</sub> H <sub>6</sub> O	94.04	0.108	
	3	2,6-Xylenol	C <sub>8</sub> H <sub>10</sub> O	122.07	4.198	
	4	Texanol	C <sub>12</sub> H <sub>24</sub> O <sub>3</sub>	216.17	0.554	
Polyphenols	5	2,4-Dihydroxytoluene	C <sub>7</sub> H <sub>8</sub> O <sub>2</sub>	124.05	0.011	
	6	2,4,6-Trihydroxytoluene	C <sub>7</sub> H <sub>8</sub> O <sub>3</sub>	140.05	0.140	
	7	Glycerol	C <sub>3</sub> H <sub>8</sub> O <sub>3</sub>	92.05	0.002	
	8	Levoglucofan	C <sub>6</sub> H <sub>10</sub> O <sub>5</sub>	162.05	0.061	
Monoacid	9	Formic acid	CH <sub>2</sub> O <sub>2</sub>	46.01	0.039	
	10	Acrylic acid	C <sub>3</sub> H <sub>4</sub> O <sub>2</sub>	72.02	0.360	
	11	Propionic acid	C <sub>3</sub> H <sub>6</sub> O <sub>2</sub>	74.04	0.150	
	12	Butyric acid	C <sub>4</sub> H <sub>8</sub> O <sub>2</sub>	88.05	0.113	
	13	n-Pentanoic acid	C <sub>5</sub> H <sub>10</sub> O <sub>2</sub>	102.07	0.069	
	14	Acetic acid	C <sub>2</sub> H <sub>4</sub> O <sub>2</sub>	60.02	0.775	
	15	Hexanoic acid	C <sub>6</sub> H <sub>12</sub> O <sub>2</sub>	116.08	0.057	
	16	2-Ethylhexanoic acid	C <sub>8</sub> H <sub>16</sub> O <sub>2</sub>	144.12	0.018	
	17	Allylacetic acid	C <sub>5</sub> H <sub>8</sub> O <sub>2</sub>	100.05	0.017	
	18	Cyanoacetic acid	C <sub>3</sub> H <sub>3</sub> NO <sub>2</sub>	85.02	0.002	
Diacid	19	Cyclopentane carboxylic acid	C <sub>6</sub> H <sub>10</sub> O <sub>2</sub>	114.07	0.127	
	20	Fumaric acid	C <sub>4</sub> H <sub>4</sub> O <sub>4</sub>	116.01	0.161	
	21	Oxalic Acid	C <sub>2</sub> H <sub>2</sub> O <sub>4</sub>	90.00	0.015	
	22	Adipic acid	C <sub>6</sub> H <sub>10</sub> O <sub>4</sub>	146.06	0.004	

	23	Phthalic acid	$C_8H_6O_4$	166.03	0.079	
	24	Glutaric acid	$C_5H_8O_4$	132.04	0.029	
	25	1,7-Heptanedicarboxylic acid	$C_9H_{16}O_4$	188.10	0.115	
Phenolic acid	26	Salicylic acid	$C_7H_6O_3$	138.03	0.013	
	27	Citric acid	$C_6H_8O_7$	192.03	0.038	
	28	Glycolic acid	$C_2H_4O_3$	76.02	0.013	
	29	lactic acid	$C_3H_6O_3$	90.03	0.006	
	30	2-hydroxy-2-methylbutyric acid	$C_5H_{10}O_3$	118.06	0.001	
Keto acid	31	Pinonic acid	$C_{10}H_{16}O_3$	184.11	0.006	
	32	Pyruvic acid	$C_3H_4O_3$	88.02	0.140	
	33	levulinic acid	$C_5H_8O_3$	116.05	0.003	
Furanone	34	3-Methyl-2(5H)-furanone	$C_5H_6O_2$	98.04	2.448	
	35	Furfural	$C_5H_4O_2$	96.02	10.391	
Others	36	Phthalic anhydride	$C_8H_4O_3$	148.02	0.259	
	37	Diethyl itaconate	$C_9H_{14}O_4$	186.09	0.091	

\* The Detection limit unit is ppb in 1-seconds, S/N=3

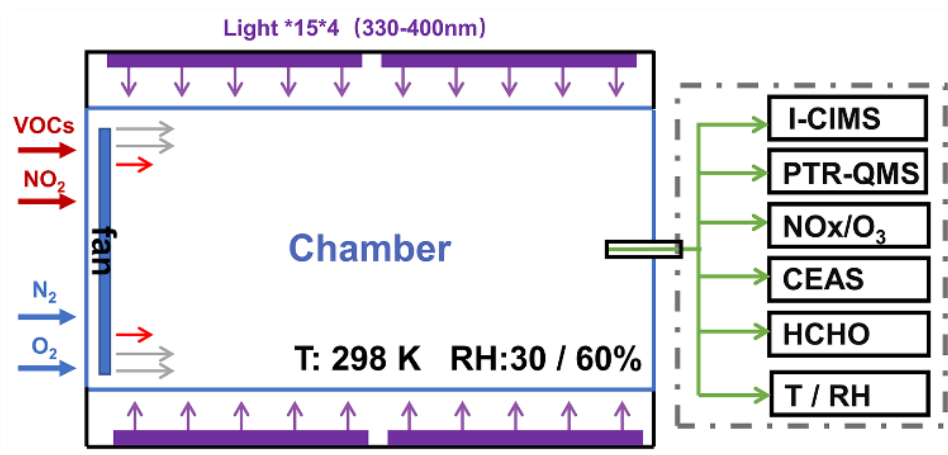


Figure S1: Schematic diagram of the chamber set up for the aromatic hydrocarbon oxidation experiment.

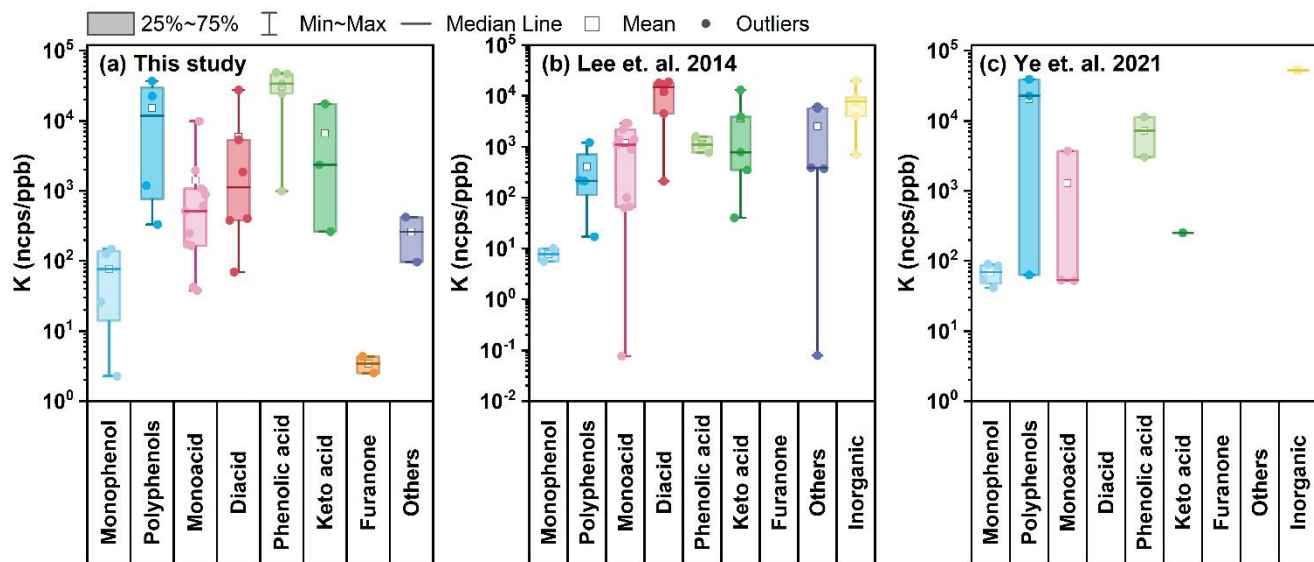


Figure S2: Comparison of the sensitivity of species containing different functional groups in (a) this study, (b) Lee et al. (Lee et al., 2014), and (c) Ye et al. (Ye et al., 2021)

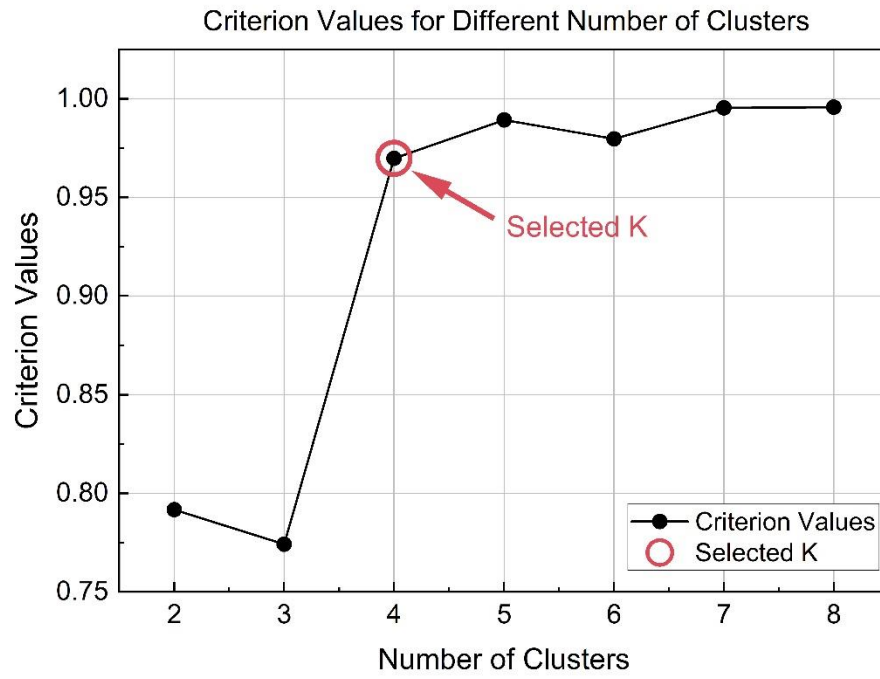


Figure S3: Criterion values for number of clusters from 2 to 8.



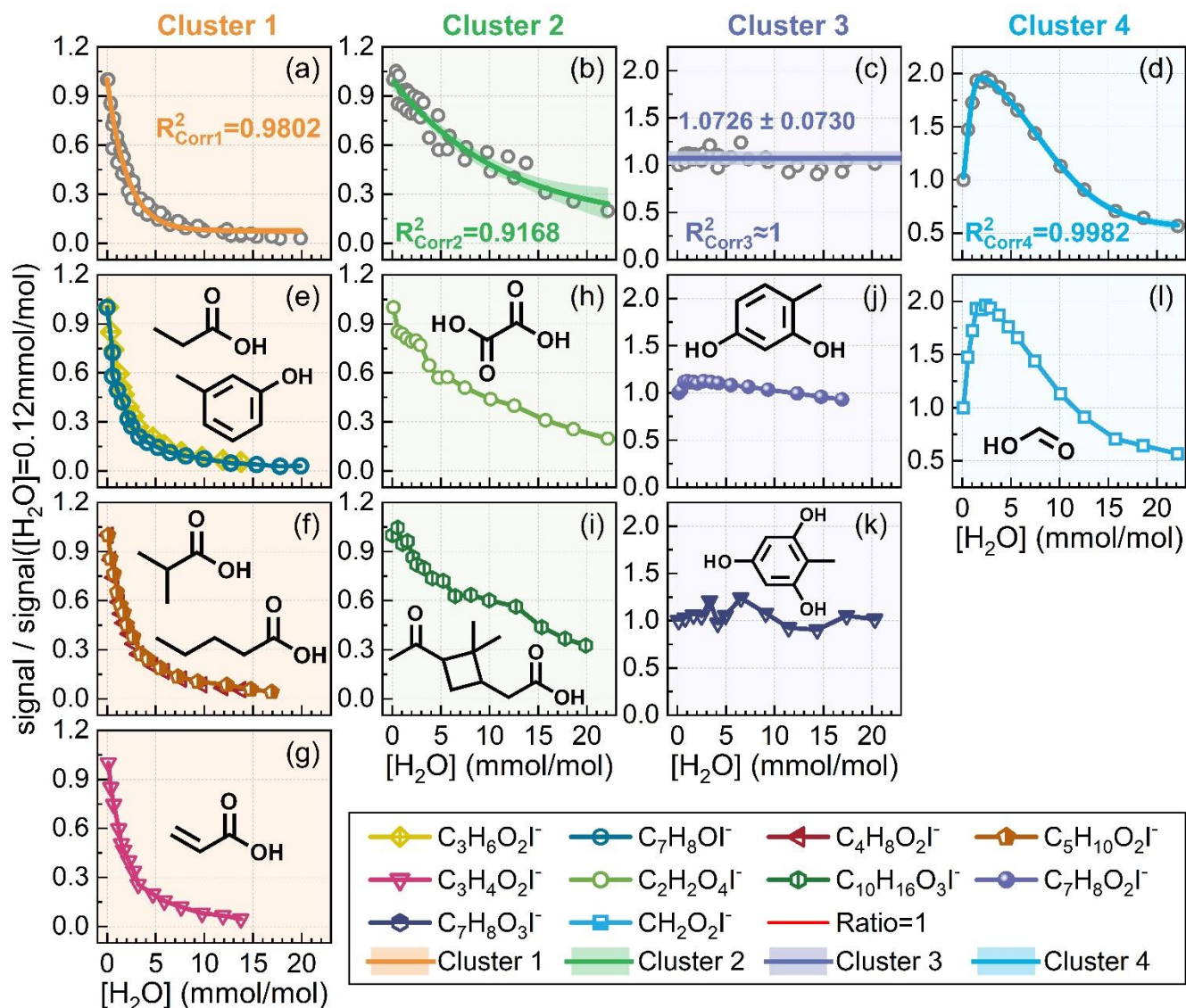


Figure S4: The effect of humidity on the sensitivity of I-CIMS. (a) Correction equation for the effects of humidity on single active functional group compounds, (b) Correction equation for the effects of humidity on compounds containing multiple active functional groups, (c) Correction equation for the effects of humidity on polyphenols, and (d) Correction equation for the effect of humidity on small molecular weight acid species (formic acid). (e) – (l) The effect of humidity on the sensitivity of different species. Note. humidity was calculated as the partial pressure of water vapor under atmospheric pressure.

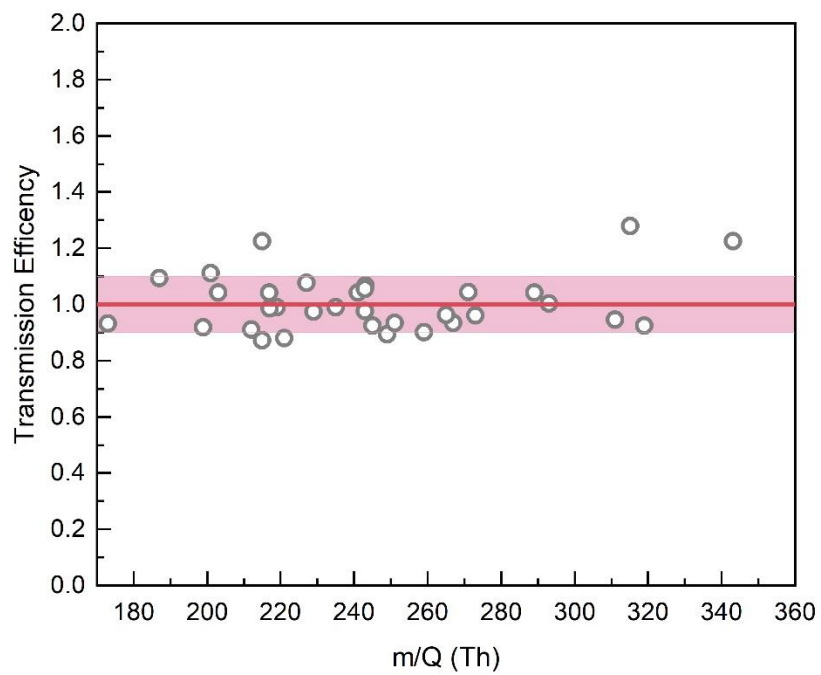


Figure S5: I-CIMS mass transmission efficiency based on direct calibration species.

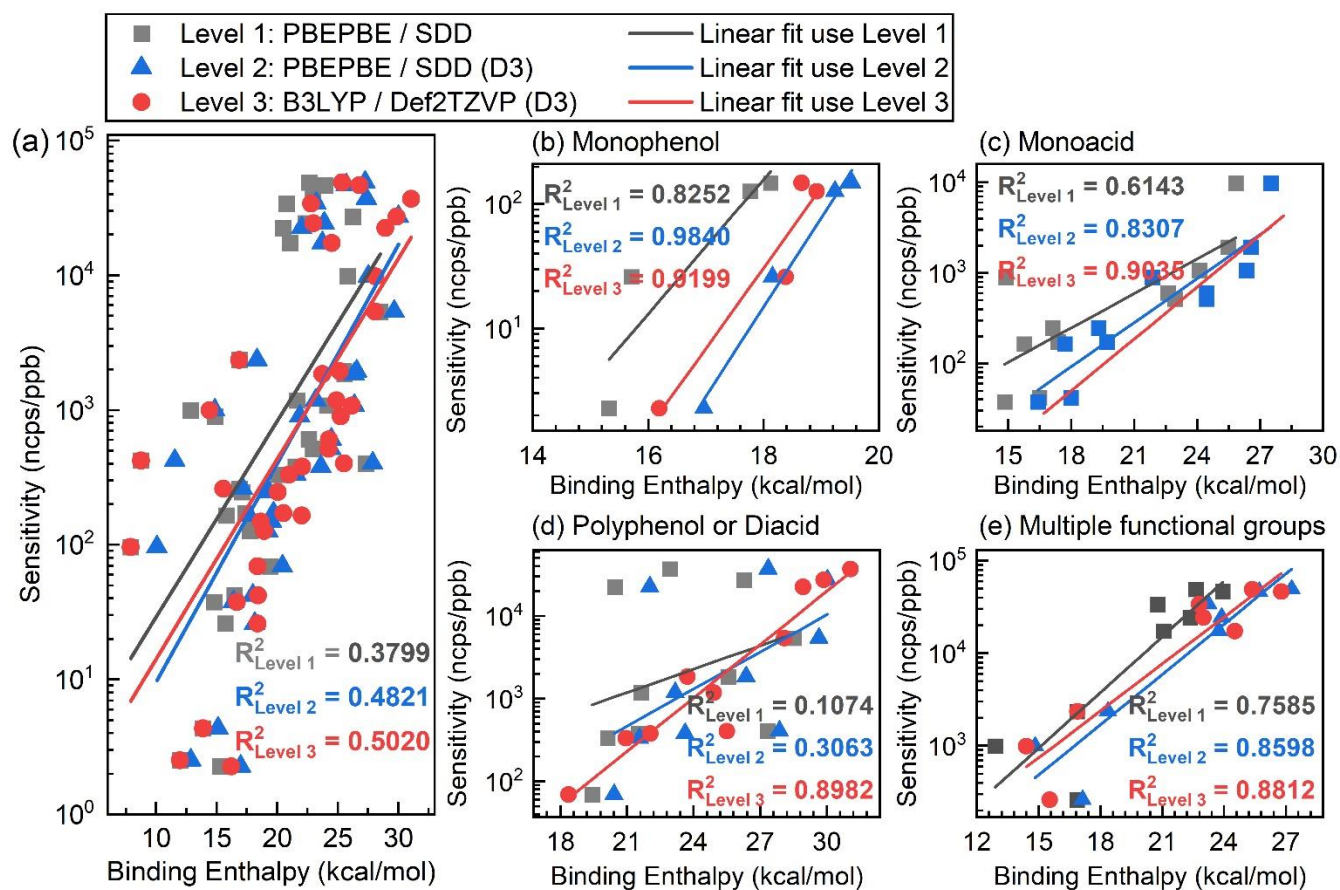


Figure S6: Fitting curve for cluster binding enthalpies and logarithmic sensitivities at PBE/SDD, PBE/SDD (D3), and B3LYP/Def2TZVP level

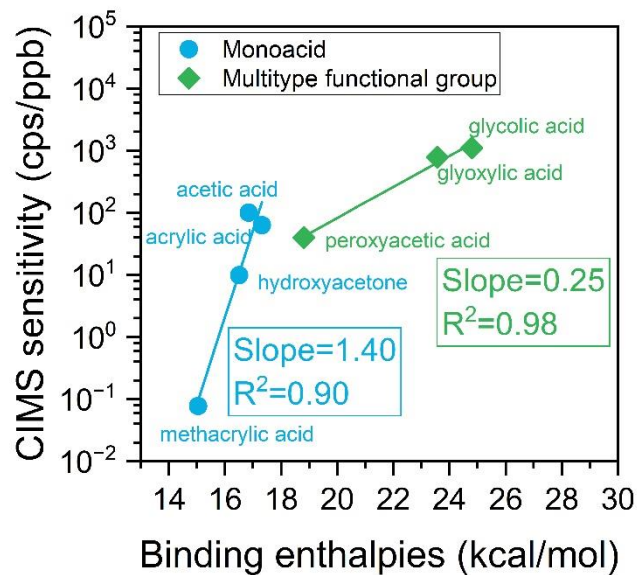
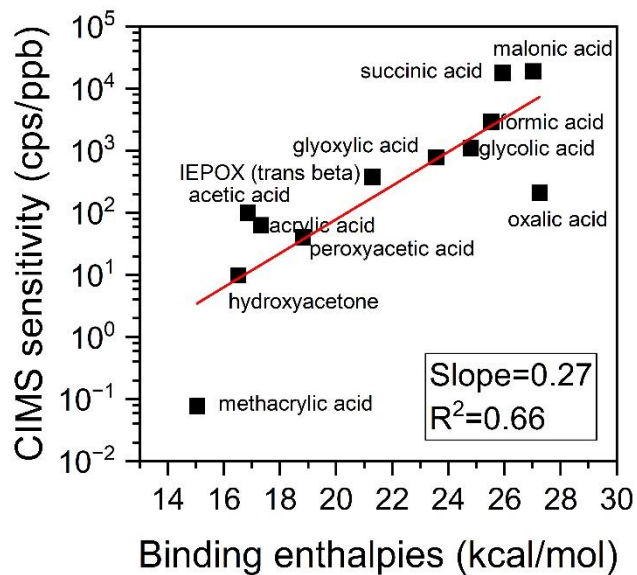
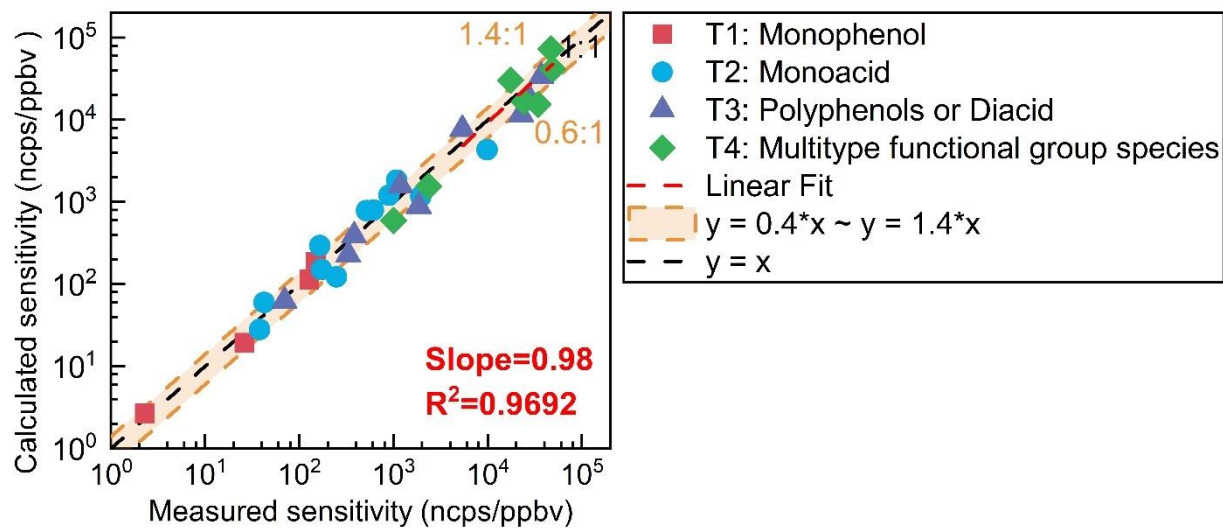
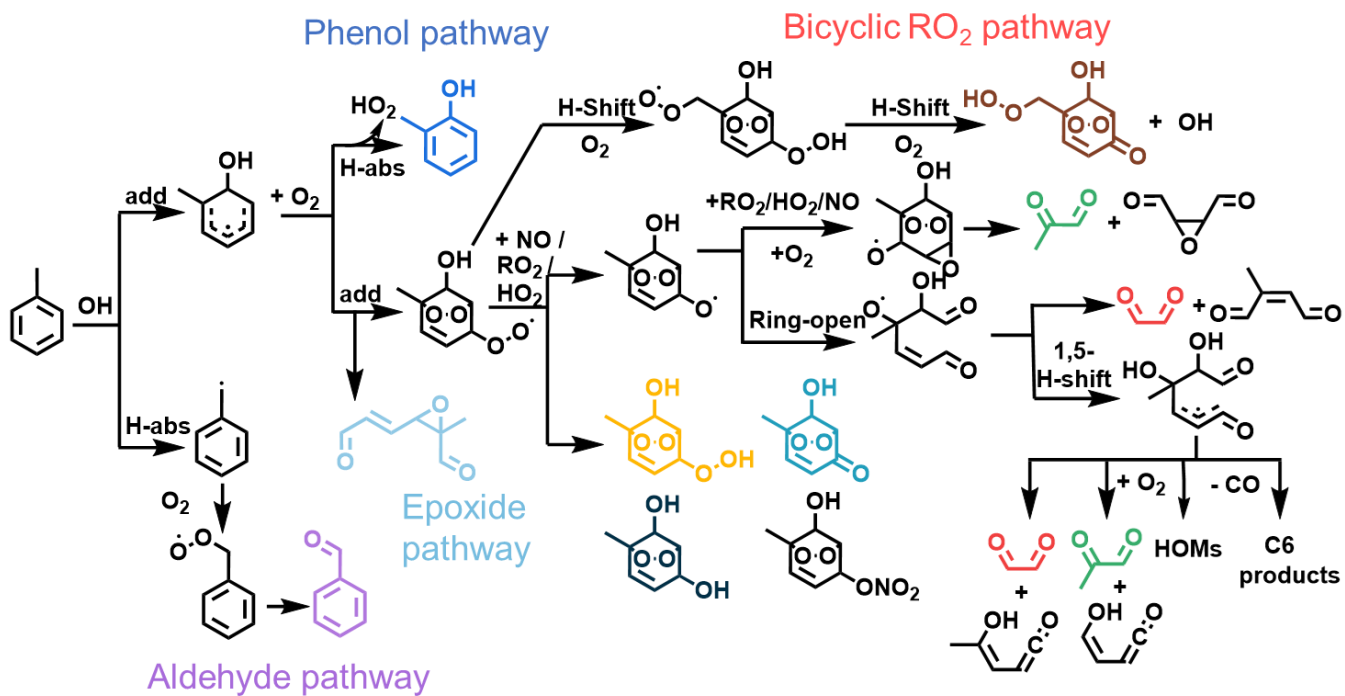


Figure S7: The application of classification-based semi-quantitative methods in previous studies (Iyer et al., 2016).

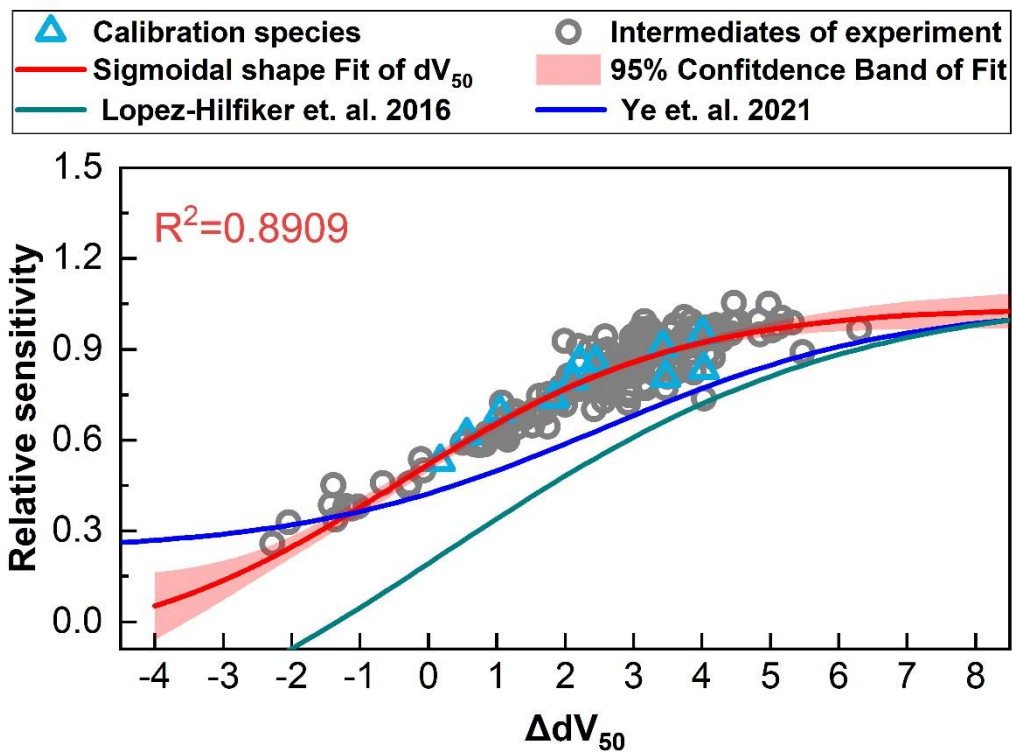


10

**Figure S8:** The difference between the measured sensitivity and the calculated sensitivity at the B3LYP/Def2TZVP (D3) level in this study.



15 Figure S9: The schematic diagram of the oxidation intermediates in the toluene + OH system.



20 **Figure S10:** Fitting results of the relative binding energy indicator  $dV_{50}$  for the iodide adducts of standard species and aromatic hydrocarbon oxidation products with the species sensitivity relative to maximum sensitivity, where  $dV_{50}$  represents the voltage at half signal maximum.

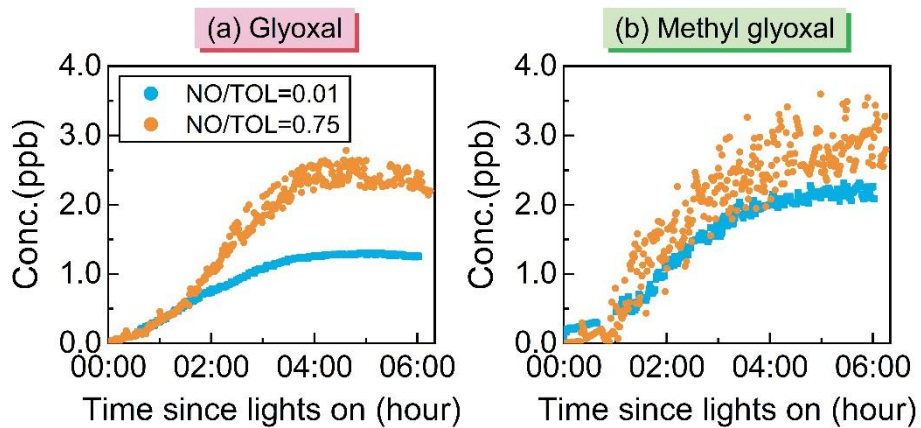


**Figure S11: Time series of (a) glyoxal and (b) methyl glyoxal during the oxidation of toluene without NO injection (blue) and with NO injection (orange). Note: glyoxal and methyl glyoxal were measured by CEAS instrument**



## References

- 30 Äijälä, M., Heikkinen, L., Fröhlich, R., Canonaco, F., Prévôt, A. S. H., Junninen, H., Petäjä, T., Kulmala, M., Worsnop, D., and Ehn, M.: Resolving anthropogenic aerosol pollution types – deconvolution and exploratory classification of pollution events, *Atmos. Chem. Phys.*, 17, 3165-3197, <https://doi.org/10.5194/acp-17-3165-2017>, 2017.
- Huang, G., Liu, Y., Shao, M., Li, Y., Chen, Q., Zheng, Y., Wu, Z., Liu, Y., Wu, Y., Hu, M., Li, X., Lu, S., Wang, C., Liu, J., Zheng, M., and Zhu, T.: Potentially Important Contribution of Gas-Phase Oxidation of Naphthalene and Methylanthalene to Secondary Organic Aerosol during Haze Events in Beijing, *Environ. Sci. Technol.*, 53, 1235-1244, <https://doi.org/10.1021/acs.est.8b04523>, 2019.
- 35 Iyer, S., Lopez-Hilfiker, F., Lee, B. H., Thornton, J. A., and Kurtén, T.: Modeling the Detection of Organic and Inorganic Compounds Using Iodide-Based Chemical Ionization, *J. Phys. Chem. A*, 120, 576-587, <https://doi.org/10.1021/acs.jpca.5b09837>, 2016.
- 40 Lee, B. H., Lopez-Hilfiker, F. D., Mohr, C., Kurten, T., Worsnop, D. R., and Thornton, J. A.: An Iodide-Adduct High-Resolution Time-of-Flight Chemical-Ionization Mass Spectrometer: Application to Atmospheric Inorganic and Organic Compounds, *Environ. Sci. Technol.*, 48, 6309-6317, <https://doi.org/10.1021/es500362a>, 2014.
- Liu, J., Li, X., Yang, Y., Wang, H., Wu, Y., Lu, X., Chen, M., Hu, J., Fan, X., Zeng, L., and Zhang, Y.: An IBBCEAS system for atmospheric measurements of glyoxal and methylglyoxal in the presence of high NO<sub>2</sub> concentrations, *Atmos. Meas. Tech.*, 12, 4439-4453, <https://doi.org/10.5194/amt-12-4439-2019>, 2019.
- 45 Liu, J., Li, X., Tan, Z., Wang, W., Yang, Y., Zhu, Y., Yang, S., Song, M., Chen, S., Wang, H., Lu, K., Zeng, L., and Zhang, Y.: Assessing the Ratios of Formaldehyde and Glyoxal to NO<sub>2</sub> as Indicators of O<sub>3</sub>-NO<sub>x</sub>-VOC Sensitivity, *Environ. Sci. Technol.*, 55, 10935-10945, <https://doi.org/10.1021/acs.est.0c07506>, 2021.
- Lopez-Hilfiker, F. D., Iyer, S., Mohr, C., Lee, B. H., D'Ambro, E. L., Kurten, T., and Thornton, J. A.: Constraining the sensitivity of iodide adduct chemical ionization mass spectrometry to multifunctional organic molecules using the collision limit and thermodynamic stability of iodide ion adducts, *Atmos. Meas. Tech.*, 9, 1505-1512, <https://doi.org/10.5194/amt-9-1505-2016>, 2016.
- Ye, C., Yuan, B., Lin, Y., Wang, Z., Hu, W., Li, T., Chen, W., Wu, C., Wang, C., Huang, S., Qi, J., Wang, B., Wang, C., Song, W., Wang, X., Zheng, E., Krechmer, J. E., Ye, P., Zhang, Z., Wang, X., Worsnop, D. R., and Shao, M.: Chemical characterization of oxygenated organic compounds in the gas phase and particle phase using iodide CIMS with FIGAERO in urban air, *Atmos. Chem. Phys.*, 21, 8455-8478, <https://doi.org/10.5194/acp-21-8455-2021>, 2021.
- 55 Yuan, B., Koss, A. R., Warneke, C., Coggon, M., Sekimoto, K., and de Gouw, J. A.: Proton-Transfer-Reaction Mass Spectrometry: Applications in Atmospheric Sciences, *Chem. Rev.*, 117, 13187-13229, <https://doi.org/10.1021/acs.chemrev.7b00325>, 2017.
- 60 Zhong, S., Zhang, K., Bagheri, M., Burken, J. G., Gu, A., Li, B., Ma, X., Marrone, B. L., Ren, Z. J., Schrier, J., Shi, W., Tan, H., Wang, T., Wang, X., Wong, B. M., Xiao, X., Yu, X., Zhu, J.-J., and Zhang, H.: Machine Learning: New Ideas and Tools in Environmental Science and Engineering, *Environ. Sci. Technol.*, 55, 12741-12754, <https://doi.org/10.1021/acs.est.1c01339>, 2021.